Universal Effective Charges in the *sd* and *fp* Shells

T. H. Ogunbeku,[1] J. M. Allmond,[2] T. J. Gray,[2,3] W.-J. Ong,[1] B. A. Brown,[4] A. Gargano,[5] R. Grzywacz,[3] J. D. Holt,[6,7] A. O. Macchiavelli,[2] T. Miyagi,[8,9,10,11] S. Neupane,[1] B. C. Rasco,[2] H. Schatz,[4,12] B. M. Sherrill,[4,12] O. B. Tarasov,[4] H. Arora,[13] A. D. Ayangeakaa,[14,15] H. C. Berg,[4,12] J. M. Berkman,[4,16] D. L. Bleuel,[1] K. Bosmpotinis,[4,12] M. P. Carpenter,[17] G. Cerizza,[4] A. Chester,[4] J. M. Christie,[3] I. Cox,[3] H. L. Crawford,[18] B. P. Crider,[19] J. Davis,[20] A. A. Doetsch,[4,12] J. G. Duarte,[1] A. Estrade,[13] A. Fijałkowska,[21] C. Frantzis,[4,12] T. Gaballah,[4,19] E. C. Good,[20] K. Haak,[4,12] S. Hanai,[22] J. T. Harke,[1] A. C. Hartley,[4,12] K. Hermansen,[4,12] D. E. M. Hoff,[1] D. Hoskins III,[3] J. Huffman,[4,12] P. Van Isacker,[23] R. Jain,[1] M. Karny,[21] T. T. King,[2] N. Kitamura,[3] K. Kolos,[1] A. Laminack,[2] S. N. Liddick,[4,16] B. Longfellow,[1] R. S. Lubna,[4] S. Lyons,[20] M. Madurga,[3] M. J. Mogannam,[4,16] G. Owens-Fryar,[4,12] J. R. Palomino,[19] M. M. Rajabali,[24] A. L. Richard,[25] I. J. Richardson,[4] E. K. Ronning,[4,16] G. E. Rose,[26] T. J. Ruland,[2] K. P. Rykaczewski,[2] N. D. Scielzo,[1] D. P. Scriven,[4] D. Seweryniak,[27] K. Siegl,[3] M. Singh,[3] A. Spyrou,[4,12] M. Stepaniuk,[21] A. E. Stuchbery,[28] A. Sweet,[1] V. Tripathi,[29] A. Tsantiri,[4,12] S. Uthayakumaar,[4] W. B. Walters,[30] S. Watters,[4,12] Z. Xu,[3] and R. Yokoyama[22]

[1]*Lawrence Livermore National Laboratory, Livermore, California 94550, USA*
[2]*Physics Division, Oak Ridge National Laboratory, Oak Ridge, Tennessee 37831, USA*
[3]*Department of Physics and Astronomy, University of Tennessee, Knoxville, Tennessee 37966, USA*
[4]*Facility for Rare Isotope Beams, Michigan State University, East Lansing, Michigan 48824, USA*
[5]*Istituto Nazionale di Fisica Nucleare, Complesso Universitario di Monte S. Angelo, Napoli I-80126, Italy*
[6]*TRIUMF, 4004 Wesbrook Mall, Vancouver, British Columbia V6T 2A3, Canada*
[7]*Department of Physics, McGill University, 3600 Rue University, Montréal, Quebec H3A 2T8, Canada*
[8]*Department of Nuclear Physics, Technische Universität Darmstadt, 64289 Darmstadt, Germany*
[9]*ExtreMe Matter Institute EMMI, GSI Helmholtzzentrum für Schwerionenforschung GmbH, 64291 Darmstadt, Germany*
[10]*Max-Planck-Institut für Kernphysik, Saupfercheckweg 1, 69117 Heidelberg, Germany*
[11]*Center for Computational Sciences, University of Tsukuba, 1-1-1 Tennodai, Tsukuba, Ibraki 305-8577, Japan*
[12]*Department of Physics and Astronomy, Michigan State University, East Lansing, Michigan 48824, USA*
[13]*Department of Physics, Central Michigan University, Mount Pleasant, Michigan 48859, USA*
[14]*Department of Physics and Astronomy, University of North Carolina at Chapel Hill, Chapel Hill, North Carolina 27599, USA*
[15]*Triangle Universities Nuclear Laboratory, Duke University, Durham, North Carolina 27708, USA*
[16]*Department of Chemistry, Michigan State University, East Lansing, Michigan 48824, USA*
[17]*Physics Division, Argonne National Laboratory, Argonne, Illinois 60439, USA*
[18]*Nuclear Science Division, Lawrence Berkeley National Laboratory, Berkeley, California 94720, USA*
[19]*Department of Physics and Astronomy, Mississippi State University, Mississippi State, Mississippi 39762, USA*
[20]*Pacific Northwest National Laboratory, Richland, Washington 99354, USA*
[21]*Faculty of Physics, University of Warsaw, PL 02-093 Warsaw, Poland*
[22]*Center for Nuclear Study, University of Tokyo, Wako, Saitama 351-0198, Japan*
[23]*Grand Accélérateur National d'Ions Lourds, CEA/DSM-CNRS/IN2P3, Boulevard Henri Becquerel, F-14076 Caen, France*
[24]*Physics Department, Tennessee Technological University, Cookeville, Tennessee 38505, USA*
[25]*Department of Physics and Astronomy, Ohio University, Athens, Ohio 45701, USA*
[26]*University of California, Berkeley, Berkeley, California 94704, USA*
[27]*Physics Division, Argonne National Laboratory, Argonne, Illinois 60439, USA*
[28]*Department of Nuclear Physics and Accelerator Applications, Research School of Physics, The Australian National University, ACT 2601, Canberra, Australia*
[29]*Department of Physics, Florida State University, Tallahassee, Florida 32306, USA*
[30]*Department of Chemistry and Biochemistry, University of Maryland, College Park, Maryland 20742, USA*

(Received 24 January 2025; accepted 23 June 2025; published 14 August 2025)

The 247-keV state in ^{54}Sc, populated in the β decay of ^{54}Ca, is reported here as a nanosecond isomer with a half-life of 26.0(22) ns. The state is interpreted as the 1^+ member of the $\pi f_{7/2} \otimes \nu f_{5/2}$ spin-coupled multiplet, which decays to the $3^+, \pi f_{7/2} \otimes \nu p_{1/2}$ ground state. The new half-life corresponds to a pure $E2$ transition with a strength of 1.93(16) W.u., providing the most precise, unambiguous $B(E2)$ value in the neutron-rich fp region to date for a nucleus with valence protons above $Z = 20$. Notably, it is roughly 4 times larger than the $B(E2; 1/2^- \to 5/2^-)$ value in ^{55}Ca. The results, as compared to semiempirical and *ab initio* shell-model calculations, indicate (1) a weak $N = 34$ subshell gap relative to $N = 32$, (2) a large $E2$ enhancement in Sc as compared to Ca due to $1p-1h$ proton excitations across $Z = 28$, and

(3) empirical effective proton and neutron charges $e_\pi = 1.30(8)e$ and $e_\nu = 0.452(7)e$, respectively, that are in contrast to reports of $e_\pi \approx 1.1$–$1.15e$ and $e_\nu \approx 0.6$–$0.8e$ for fp-shell nuclei near $N = Z$. We demonstrate that these reports are erroneous and that, in fact, a universal set of effective charges can be used across the sd and fp shells.

DOI: 10.1103/75ry-71sj

The nuclear shell model provides a fundamental view of nuclear structure [1,2]. It presumes independent particle motion in a spherical mean field with strong spin-orbit coupling, leading to significant energy gaps at "magic" proton and neutron numbers, $Z, N = 2, 8, 20, 28, 50, 82$, and 126. Modeling nuclear structure then involves understanding the correlations or effective interactions between valence nucleons, which mix single-particle configurations, within a finite, truncated model space. However, exotic nuclei with increasing neutron excess relative to stable nuclei become sensitive to different aspects of the nuclear forces [3–6]. This leads to an evolution of the single-particle orbitals, causing standard magic numbers to disappear and new ones to emerge [7,8]. All effects from outside of the truncated model space are then treated with effective operators, which have been reported to have isospin and orbital dependencies beyond the sd shell [9,10].

Considerable interest has been directed toward the emergence of new subshell gaps at $N = 32$ and 34 in neutron-rich nuclei within the fp shell. These gaps are currently understood to be driven by the elevation of the $\nu 1f_{5/2}$ orbital as protons are removed from the $\pi 1f_{7/2}$ orbital. The existence of the $N = 32$ subshell gap has been extensively confirmed near $Z = 20$ by the measurement of high $E(2_1^+)$ values in ^{50}Ar [11], ^{52}Ca [12,13], ^{54}Ti [14,15], and ^{56}Cr [16–18]. These findings have been further supported by mass measurements of $^{51–54}$Ca [19,20], ^{52,53}K [21], and $^{52–54}$Sc [22,23]. However, mass measurements of Ti and V isotopes [24,25] have introduced some ambiguity.

The $N = 34$ subshell closure is less clear. Initial evidence came from ^{54}Ca, where a high $E(2_1^+)$ of 2043(19) keV was measured [26]. This was further supported by direct mass measurements of $^{55–57}$Ca [27]. In ^{52}Ar, the 2_1^+ state was measured at 1656(18) keV [28]. Spectroscopic strengths from knockout reactions supported subshell closures at $N = 32$ and $N = 34$ [29,30]. However, the persistence of the $N = 34$ subshell gap above $Z = 20$ remains uncertain [15,25,31–35].

Another point of interest for the region is the unexpectedly large charge radii of $^{49–52}$Ca [36], where neutron filling shifts from the $\nu 1f_{7/2}$ to the $\nu 2p_{3/2}$ orbital. The sudden rise beyond $N = 28$ is striking given the equivalent charge radii of ^{40}Ca and ^{48}Ca. In fact, the isotope shifts between ^{40}Ca and ^{48}Ca seem to be described solely by the $E2$ strength [37]. The change in charge radii beyond $N=28$ has been attributed to core polarization and a p-orbit halo, both of which can induce neutron skins [38]. The effective neutron charge, determined from a $B(E2; 2^+ \to 0^+)$ measurement in ^{50}Ca, also showed a sudden change with the occupation of the $\nu 2p_{3/2}$ orbital [9]. A comparable result was reported from inelastic proton scattering on ^{50}Ca [39].

In this Letter, we investigate ^{54}Sc by decay spectroscopy at the Facility for Rare Isotope Beams (FRIB) using the FRIB Decay Station initiator (FDSi) [40,41]. ^{54}Sc is positioned one proton above the $Z = 20$ shell closure and one neutron between the $N = 32$, 34 subshell closures. This gives rise to relatively simple single proton-neutron (PN) coupled states at low excitation energies that are sensitive to the magnitudes of the $N = 32$, 34 subshell gaps. A new nanosecond isomer is reported that corresponds to the most precise, unambiguous $E2$ transition strength in the neutron-rich fp region to date in a nucleus with valence protons above $Z = 20$. The new B($E2$) value and resulting effective charges provide a unique opportunity to probe core-polarization effects in neutron-rich fp-shell nuclei near $N = 32$, 34.

The present results are from two experiments conducted at FRIB using the two-focal-plane configuration of the FDSi. In both experiments, a secondary cocktail beam of fully stripped ions produced in the fragmentation reaction between an ^{82}Se primary beam and a ^{9}Be target were delivered to the FDSi. At the first focal plane, γ rays and neutrons were detected using the DEcay Germanium Array initiator and the Versatile Array of Neutron Detectors at Low Energy [42,43], respectively. The Modular Total Absorption Spectrometer (MTAS) [44,45] was situated at the second focal plane. At both focal planes, cocktail beams centered around ^{52,54}K were implanted within a position-sensitive yttrium orthosilicate (YSO) detector [46,47]. See Refs. [48–50] for additional experimental details.

The γ rays observed following the β decay of ^{54}Ca and implantation of ^{54m}Sc are presented in Figs. 1(a) and 1(b), respectively. The 247-keV β-delayed γ-ray transition, identified in this work with an absolute intensity of 62(8)%, was previously reported in Refs. [51,52]. The transition was attributed to a 247-keV state in ^{54}Sc with a spin parity of $J^\pi = 1^+$ based on the selectivity of the 0^+ parent decay. The statistics of the present work are higher by an order of magnitude than Ref. [52], but no additional discrete γ rays in ^{54}Sc were observed.

The fast-timing capabilities of the YSO and $LaBr_3$ scintillators at the first focal plane of the FDSi have

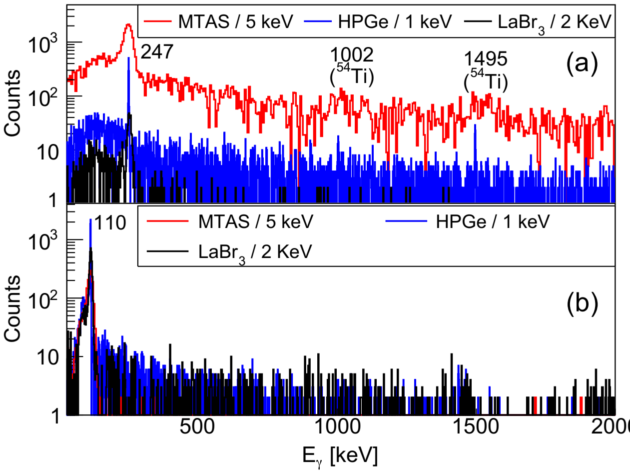

FIG. 1. (a) β-delayed γ-ray spectra measured within 300 ms of ^{54}Ca ion implantation. (b) γ-ray spectra collected within 20 μs of ^{54m}Sc implantation.

enabled the identification of the 247-keV, 1^+ state in ^{54}Sc as a nanosecond isomer, as shown in Fig. 2. A maximum-likelihood fit to the β-γ time difference distribution yielded a $26.0(22)_{\mathrm{stat}}(3)_{\mathrm{sys}}$ ns half-life. The fit incorporated an exponentially modified Gaussian function with a background distribution derived from regions adjacent to the 247-keV peak.

The presence of a low-lying microsecond isomer in ^{54}Sc was initially reported in Ref. [53] with $J^\pi = (4^+, 5^+)$, and confirmed [15,52] based on the detection of a 110-keV γ-ray peak following ^{54m}Sc implantation. In this work, the microsecond ^{54m}Sc isomer is confirmed as shown in Fig. 1(b) and no additional γ rays are observed in association with its decay. A fit to the implant-γ time-difference distributions yielded half-lives of 2.74(4), 2.80(6), and 2.72(9) μs for the HPGe, $LaBr_3$, and MTAS detectors, respectively. The weighted average, 2.75(3) μs, agrees with previous values of 7(5) μs [53] and 2.77(2) μs [52].

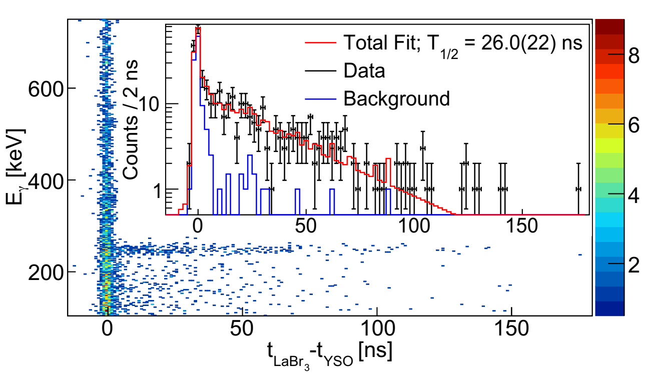

FIG. 2. β-γ time-difference distribution as a function of γ-ray energy in the $LaBr_3$ detectors following ^{54}Ca implantation. Inset: time-difference distribution corresponding to a 247-keV energy gate.

The low-lying states of ^{54}Sc can be schematically interpreted with respect to a ^{52}Ca ($Z = 20$, $N = 32$) core, outside of which the odd $7/2^-$ proton from ^{53}Sc and odd $1/2^-$ neutron from ^{53}Ca spin couple to a 3^+, 4^+ doublet. The population of the first 2^+ and 4^+ states in ^{54}Ti following the β decay of ^{54}Sc supports a 3^+ ground-state assignment for ^{54}Sc, consistent with discussions in Refs. [15,51,52]. Furthermore, this population is identical between the $^{54}\mathrm{Sc} \to {}^{54}\mathrm{Ti}$ and $^{54}\mathrm{Ca} \to {}^{54}\mathrm{Sc} \to {}^{54}\mathrm{Ti}$ decay chains, suggesting the absence of a β-decaying isomer. The next lowest multiplet of states would then arise from a single-particle neutron excitation across $N = 34$, corresponding to the excited $5/2^-$ state in ^{53}Ca coupled to the $7/2^-$ ground state in ^{53}Sc. The $\pi f_{7/2} \otimes \nu f_{5/2}$ coupling forms a sextet of states with $J^\pi = 1^+ - 6^+$.

The 247-keV γ ray deexciting the nanosecond isomer corresponds to a $1^+ \to 3^+$ transition between the two multiplets with an experimental $B(E2)$ of $1.93(16)_{\mathrm{stat}}(2)_{\mathrm{sys}}$ W.u. determined in this work. The 110-keV γ ray deexciting the microsecond isomer may represent either (a) a pure $2^+ \to 4^+$ or $6^+ \to 4^+$ $E2$ transition between the two multiplets with $B(E2) = 0.86(1)$ W.u., or (b) a mixed $4^+ \to 3^+$ $E2/M1$ transition within the $\pi f_{7/2} \otimes \nu p_{1/2}$ multiplet with $B(M1) \leq 5.92(7) \times 10^{-6}$ W.u. and $B(E2) \leq 0.86(1)$ W.u. We adopt the latter, which is consistent with discussions in Ref. [52], as the 2^+ and 6^+ states are expected to lie well above the antiparallel 1^+ state, and the in-multiplet $M1$ transition is expected to be strongly hindered; the strength to first order is given by $B(M1; 4^+ \to 3^+) \approx (21/64\pi)(g^\pi_{f_{7/2}} - g^\nu_{p_{1/2}})^2 = 8.4 \times 10^{-3}$ W.u.

Differences in neutron separation energies along the Ca isotopic chain, which emphasize the magnitude of the shell gaps, and level schemes for ^{54}Sc are shown in Figs. 3(a) and 3(b), respectively. Predictions by the KB3G [54] and GXPF1A [55] interactions, used in previous ^{54}Sc studies, are compared with recent UFP-CA (empirically adjusted) [56], SM* (perturbative *ab initio*) [57,58], and VS-IMSRG 1.8/2.0 EM (*ab initio*) [59–61] interactions. The UFP-CA Hamiltonian for the $T = 1$ neutron-neutron interaction was obtained from constraints to data for the Ca isotopes [56]. For application to the Sc isotopes, the $T = 0$ part of the GXPF1A Hamiltonian [55] was added. The $T = 1$ part of the GXPF1A Hamiltonian was obtained from energy data for nuclei toward the middle of the fp shell. Thus, the $T = 1$ parts of the UFP-CA and GXPF1A interactions are nucleus-dependent and the UFP-CA Hamiltonian should only be used for nuclei near $Z = 20$ with $N > 28$. All calculations were performed with KSHELL [62] in the full fp model space. For the SM* interaction, the neutron $g_{9/2}$ orbit was also included. The KB3G and GXPF1A interactions predict $N = 34$ gaps for Ca that are nonexistent and too strong, respectively, as shown in Fig. 3(a). The sensitivity of the low-energy structure of ^{54}Sc to the magnitude of the $N = 34$ gap is

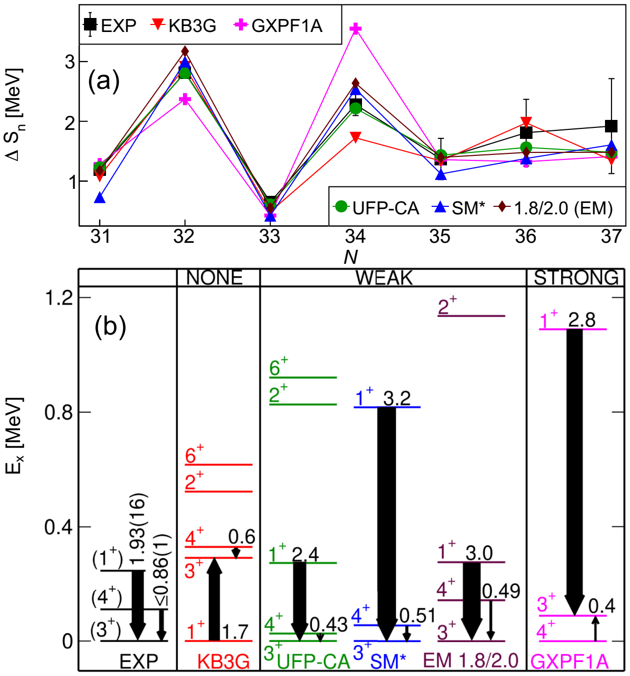

FIG. 3. Comparison of experimental and theoretical (a) neutron shell gaps along the Ca isotopic chain and (b) energy levels of ^{54}Sc. Theoretical interactions are grouped based on their predictions of the strength of the subshell gap at $N = 34$. The $B(E2)$ strengths are given in W.u. and calculated with $e_\pi = 1.5e$, $e_\nu = 0.5e$.

reflected in the two corresponding level schemes, namely a $1^+, \pi f_{7/2} \otimes \nu f_{5/2}$ state that is too low or too high, as illustrated in Fig. 3(b). The recent interactions (UFP-CA, SM*, and VS-IMSRG 1.8/2.0 EM) predict a weak $N = 34$ gap relative to $N = 32$ and better describe the experimental data and schematic interpretations. We note that the $B(E2; 1^+ \to 3^+)$ strengths predicted by the empirically adjusted interactions (KB3G, UFP-CA, and GXPF1A) also increase with the magnitude of the $N = 34$ gap and that the value for UFP-CA, which best describes the level energies, is larger than experiment.

The UFP-CA results are further investigated in Fig. 4 as a function of the PN interaction strength. All PN two-body matrix elements were multiplied by a scale parameter, V_{PN} scale. In the weak coupling limit (V_{PN} scale $= 0$), the energies (and transitions) correspond to the excited neutron states in ^{53}Ca and the excited proton states in ^{53}Sc. As the PN strength increases, each multiplet splits and begins to mix with nearby configurations. At V_{PN} scale $= 0$, $B(E2; 1_1^+ \to 3^+_{\mathrm{g.s.}})$ corresponds to the ^{53}Ca $B(E2; f_{5/2} \to p_{1/2})$. The experimentally known $B(E2; 1/2^- \to 5/2^-)$ of ^{55}Ca [63] is shown as a proxy for this limit, represented by the red band in Fig. 4(b). The PN interaction, at its nominal value (V_{PN} scale $= 1$), increases the $E2$ strength by a factor of 4. The large increase arises primarily from mixing with the second 1^+

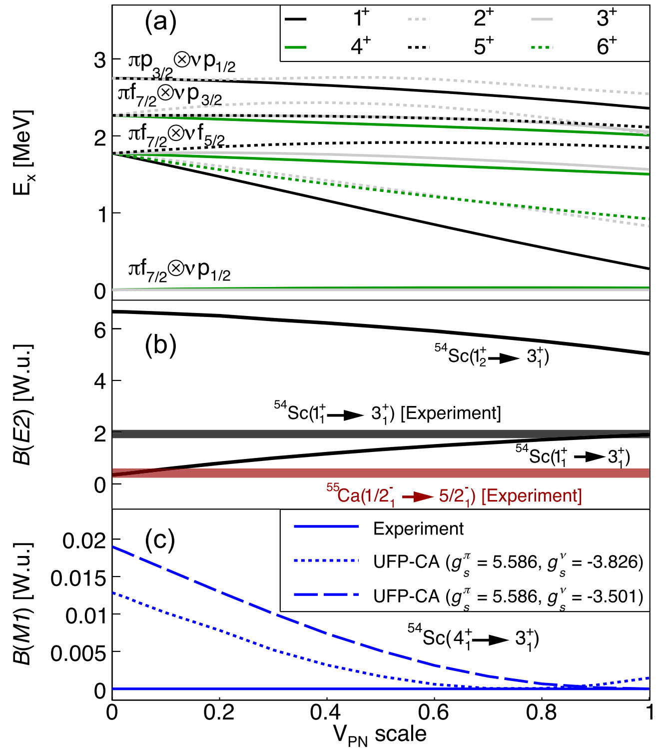

FIG. 4. UFP-CA calculations of ^{54}Sc as a function of PN strength for (a) the first four PN spin-coupled multiplets, and (b) the $B(E2)$ values with newly fitted effective charges $e_\pi = 1.30e$, $e_\nu = 0.452e$. (c) $B(M1; 4^+ \to 3^+)$ values with free and quenched spin g factors.

configuration from the $\pi p_{3/2} \otimes \nu p_{1/2}$ multiplet, where proton $p_{3/2} \to f_{7/2}$ transitions across $Z = 28$ have large intrinsic $E2$ strength. Note the large $B(E2; 1_2^+ \to 3_1^+)$ strength in the weak-coupling limit, and that the sum with $B(E2; 1_1^+ \to 3_1^+)$ remains relatively constant with the PN strength. The magnitudes of the $Z = 28$ and $N = 34$ gaps control the proximity of the two 1^+ configurations and therefore the mixing strength.

The $B(M1; 4^+ \to 3^+)$ strength vanishes completely with either small adjustments to the PN interaction strength or 0.915 attenuation of the free neutron g_s value; the total attenuation could be larger if the free proton g_s were to be attenuated. However, the ground-state magnetic dipole moments of ^{49,51}Ca, which do not depend on the proton g_s, fit best to a neutron g_s attenuation of 0.957.

A survey of $E2$ data for neutron-rich Ca, Sc, and Ti isotopes is provided in Table I, including UFP-CA predictions with the “standard” isoscalar core-polarization effective charges of $e_\pi = 1.5e$, $e_\nu = 0.5e$, and newly fitted effective charges of $e_\pi = 1.30(8)e$, $e_\nu = 0.452(7)e$. Significantly larger effective charges would have been found if $1p - 1h$ excitations across $Z = 28$ or $N = 28$ were not included, cf. Fig. 4(b) and Refs. [64,65]. The Blomqvist and Molinari oscillator parameter, $\hbar\omega = 45A^{-1/3} - 25A^{-2/3}$ [66], was used for all the

TABLE I. Experimental $E2$ strengths of neutron-rich fp-shell isotopes near $N = 32, 34$ [9,33,63,67] compared with theoretical predictions using the UFP-CA interaction with the standard ($e_\pi = 1.5e$, $e_\nu = 0.5e$) and fitted ($e_\pi = 1.30e$, $e_\nu = 0.452e$) effective charges.

		B($E2$) [W.u.] or Q [eb]		
Isotope	$J_i^\pi \to J_f^\pi$	Experiment	UFP-CA (1.5, 0.5)	UFP-CA (1.3, 0.452)
^{49}Ca	$(3/2)^-_{\mathrm{g.s}}$	−0.036(3)	−0.043	−0.039
^{50}Ca	$2_1^+ \to 0_1^+$	0.68(2)	0.82	0.68
^{51}Ca	$(3/2)^-_{\mathrm{g.s}}$	+0.036(12)	+0.042	+0.038
^{55}Ca	$½_1^- \to (5/2)_1^-$	0.42(18)	0.26	0.21
^{51}Sc	$(11/2)_1^- \to (7/2)_1^-$	1.9(5)	1.65	1.34
^{54}Sc	$1_1^+ \to 3_1^+$	1.93(16)	2.44	1.91
^{54}Ti	$2_1^+ \to 0_1^+$	6.0(12)	8.56	6.57
$\tilde{\chi}^2$			18.1	1.1

calculations, where $B(E2) \propto \langle r^2 \rangle e^2_{\pi,\nu} \propto \hbar^2\omega^2 e^2_{\pi,\nu}$. Had $\hbar\omega' = 41A^{-1/3}$ been used, the extracted effective charges would scale up by $\hbar\omega'/\hbar\omega = 1.068$. The new effective charges improve the description of the $E2$ data in Table I from a reduced chi-squared, $\tilde{\chi}^2$, of 18.1 to 1.1. The new effective neutron charge, e_ν, is qualitatively consistent with $\sim 0.5e$ reported in Ref. [9] from the $B(E2; 0^+ \to 2^+)$ of ^{50}Ca but now includes fitting to the precise ground-state quadrupole moments of ^{49,51}Ca [67]. The new e_π/e_ν ratio of 2.88(18), which is independent of $\hbar\omega$, is also consistent with 3.5(9) from inelastic proton scattering results on ^{50}Ca [39], but is now more precise by a factor of 5.

The new effective charges differ significantly from those previously established in the fp shell. For example, effective charges of $e_\pi = 1.15e$, $e_\nu = 0.8e$ (ratio of 1.44) were determined for ^{51}Fe/^{51}Mn at $N \approx Z$ in the fp shell [68], and later updated to $e_\pi = 1.12e$, $e_\nu = 0.67e$ (ratio of 1.67) to best describe the stable $N = 28$ and $Z = 28$ chains [69]. The new values are also different from $e_\pi = 1.1e$, $e_\nu = 0.6e$ (ratio of 1.83) used recently to describe ^{49,50}Ti [70]. It has been argued that changes in the effective charges across the fp shell are due to an isospin or orbital dependence [9]. However, it is worth noting that the previous and new effective charges all have similar sums, namely $e_\pi + e_\nu \approx 1.7e$–$1.95e$.

The $E2$ data and effective charges can be linearly systematized by plotting A_n/M_p versus A_p/M_p, as shown in Fig. 5. All data points should fall on a straight line with slope e_π/e_ν and intercept $1/e_\nu$ [64]. A_p and A_n represent the calculated transition amplitudes, which relate to the $E2$ matrix element by $\langle J_f^\pi || E2 || J_i^\pi \rangle = A_p e_\pi + A_n e_\nu$. M_p is the experimental $E2$ matrix element, where $B(E2) = M_p^2/(2J_i + 1)$. J_f^π and J_i^π denote the spin parity of the final and initial states, respectively. Figure 5 shows that a large majority of fp-shell nuclei, including those at $N = 28$, have $A_p \approx A_n$ meaning they are mostly sensitive to the sum of effective charges as opposed to the ratio. All of the previous cases are consistent with the new effective charges of $e_\pi = 1.30(8)e$, $e_\nu = 0.452(7)e$. These values are equivalent to the universal effective charges in the sd shell, $e_\pi = 1.36(5)e$ and $e_\nu = 0.45(5)e$ [71]. Further, they are equivalent to microscopic derivations by Dufour and Zuker, $e_\pi = 1.31e$ and $e_\nu = 0.46e$ [72], which have been applied to sd [73], sd-pf [74], pf [75], fpg_9d_5 [76], and pf-sdg [77] valence spaces. Therefore, universal effective charges of $e_\pi = 1.33e$, $e_\nu = 0.45e$, based on empirical fits, can be used across the sd and fp shells.

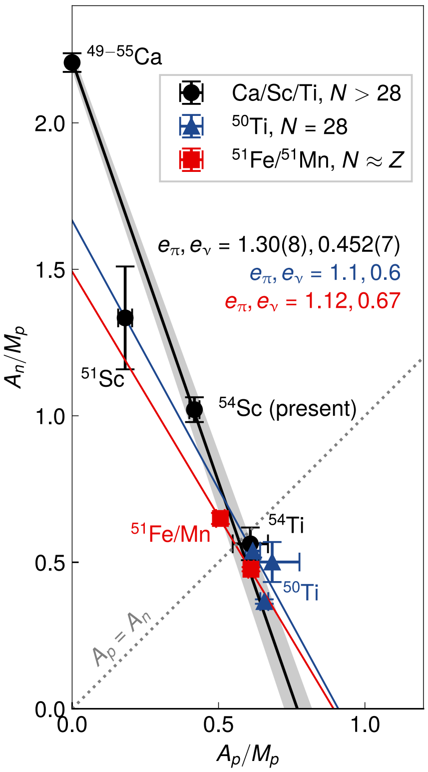

FIG. 5. Neutron versus proton transition amplitudes relative to the experimental $E2$ matrix elements for fp-shell nuclei listed in Table I [black line, $e_\pi = 1.30(8)e$, $e_\nu = 0.452(7)e$]. Additional data points represent transitions in ^{50}Ti ($N = 28$) and ^{51}Fe/^{51}Mn ($N \approx Z$) [68–70] with lines representing previously adopted effective charges. The proton amplitudes are zero for the Ca isotopes so the weighted average was adopted. See Table II in End Matter for more details.

In summary, the structure of neutron-rich ^{54}Sc is reported from two experiments at FRIB using the FDSi. The 247-keV 1^+ state was identified as a nanosecond isomer while the previously known microsecond isomer was interpreted as a $4^+ \to 3^+$ transition between the $\pi f_{7/2} \otimes \nu p_{1/2}$ spin-coupled multiplet members. The new 1^+ lifetime and resulting effective charge analysis demonstrates that a universal set of effective charges can be used across the *sd* and *fp* shells, which should enable more consistent and accurate electric-quadrupole transition and moment calculations for a large number of atomic nuclei. No evidence for changes in the effective charges due to an isospin or orbital dependence is found.

Acknowledgments—This material is based upon work supported in part by the U.S. Department of Energy, Office of Science, Office of Nuclear Physics under Contracts No. DE-AC02-06CH11357 (ANL), No. DE-AC02-98CH10946 (BNL), No. DE-AC02-05CH11231 (LBNL), No. DE-AC52-07NA27344 (LLNL), No. DE-SC0020451, No. DE-SC0023633 (Michigan State), No. DE-SC0014448 (Mississippi State), No. DE-AC05-00OR22725 (ORNL), and No. DE-FG02-96ER40983 (UTK). This work was also supported by the U.S. National Science Foundation under Grants No. PHY-23-10078, No. PHY-2110365, No. PHY-2012522 (FSU), and No. PHY-1848177 (CAREER) (Mississippi State). Additional support was provided by the U.S. Department of Energy, National Nuclear Security Administration under Award No. DE-NA0003180 (Michigan State) and the Stewardship Science Academic Alliances program through DOE Awards No. DE-NA0003899 (UTK), No. DE-SC0016988 (TTU), and No. DOE-DE-NA0003906 (Michigan State), and National Science Foundation Major Research Instrumentation Program Award No. 1919735 (UTK, TTU). This research was also supported by the Laboratory Directed Research and Development Program at Pacific Northwest National Laboratory operated by Battelle for the U.S. Department of Energy. This work was also supported in part by the Deutsche Forschungsgemeinschaft (DFG, German Research Foundation)—Project-ID 279384907—SFB 1245. This work was in part supported by the European Research Council (ERC) under the European Union's Horizon 2020 research and innovation programme (Grant Agreement No. 101020842) and JST ERATO Grant No. JPMJER2304, Japan. For the VS-IMSRG calculations, the NuHamil [79], IMSRG++ [61], and KSHELL [62] codes were used to generate chiral effective field theory matrix elements, to perform the valence-space decoupling, and to solve the valence-space problems, respectively. The VS-IMSRG calculations were in part performed with an allocation of computing resources at the Jülich Supercomputing Center and on Cygnus and Pegasus at the CCS, University of Tsukuba. This research used resources of the Facility for Rare Isotope Beams, which is a DOE Office of Science User Facility.

The publisher acknowledges the U.S. government license to provide public access under the DOE Public Access Plan [78].

Data availability—The data that support the findings of this Letter are openly available [80].

[1] M. G. Mayer, Phys. Rev. **75**, 1969 (1949).
[2] O. Haxel, J. H. D. Jensen, and H. E. Suess, Phys. Rev. **75**, 1766 (1949).
[3] D. Warner, Nature (London) **430**, 517 (2004).
[4] J. Dobaczewski, N. Michel, W. Nazarewicz, M. Płoszajczak, and J. Rotureau, Prog. Part. Nucl. Phys. **59**, 432 (2007).
[5] W. Satuła, M. Zalewski, J. Dobaczewski, P. Olbratowski, M. Rafalski, T. R. Werner, and R. A. Wyss, Int. J. Mod. Phys. E **18**, 808 (2009).
[6] T. Otsuka, A. Gade, O. Sorlin, T. Suzuki, and Y. Utsuno, Rev. Mod. Phys. **92**, 015002 (2020).
[7] T. Otsuka, T. Suzuki, R. Fujimoto, H. Grawe, and Y. Akaishi, Phys. Rev. Lett. **95**, 232502 (2005).
[8] T. Otsuka, T. Suzuki, M. Honma, Y. Utsuno, N. Tsunoda, K. Tsukiyama, and M. Hjorth-Jensen, Phys. Rev. Lett. **104**, 012501 (2010).
[9] J. J. Valiente-Dobón *et al.*, Phys. Rev. Lett. **102**, 242502 (2009).
[10] A. Jungclaus *et al.*, Phys. Rev. Lett. **132**, 222501 (2024).
[11] D. Steppenbeck *et al.*, Phys. Rev. Lett. **114**, 252501 (2015).
[12] A. Huck, G. Klotz, A. Knipper, C. Miehé, C. Richard-Serre, G. Walter, A. Poves, H. L. Ravn, and G. Marguier, Phys. Rev. C **31**, 2226 (1985).
[13] A. Gade, R. V. F. Janssens, D. Bazin, R. Broda, B. A. Brown, C. M. Campbell, M. P. Carpenter, J. M. Cook, A. N. Deacon, D.-C. Dinca, B. Fornal, S. J. Freeman, T. Glasmacher, P. G. Hansen, B. P. Kay, P. F. Mantica, W. F. Mueller, J. R. Terry, J. A. Tostevin, and S. Zhu, Phys. Rev. C **74**, 021302(R) (2006).
[14] R. V. F. Janssens *et al.*, Phys. Lett. B **546**, 55 (2002).
[15] S. N. Liddick *et al.*, Phys. Rev. C **70**, 064303 (2004).
[16] J. I. Prisciandaro, P. F. Mantica, B. A. Brown, D. W. Anthony, M. W. Cooper, A. Garcia, D. E. Groh, A. Komives, W. Kumarasiri, P. A. Lofy, A. M. Oros-Peusquens, S. L. Tabor, and M. Wiedeking, Phys. Lett. B **510**, 17 (2001).
[17] P. F. Mantica, A. C. Morton, B. A. Brown, A. D. Davies, T. Glasmacher, D. E. Groh, S. N. Liddick, D. J. Morrissey, W. F. Mueller, H. Schatz, A. Stolz, S. L. Tabor, M. Honma, M. Horoi, and T. Otsuka, Phys. Rev. C **67**, 014311 (2003).
[18] A. Bürger *et al.*, Phys. Lett. B **622**, 29 (2005).
[19] A. T. Gallant *et al.*, Phys. Rev. Lett. **109**, 032506 (2012).
[20] F. Wienholtz *et al.*, Nature (London) **498**, 346 (2013).
[21] M. Rosenbusch *et al.*, Phys. Rev. Lett. **114**, 202501 (2015).
[22] X. Xu *et al.*, Chin. Phys. C **39**, 104001 (2015).
[23] X. Xu *et al.*, Phys. Rev. C **99**, 064303 (2019).
[24] E. Leistenschneider *et al.*, Phys. Rev. Lett. **120**, 062503 (2018).
[25] W. S. Porter *et al.*, Phys. Rev. C **106**, 024312 (2022).
[26] D. Steppenbeck *et al.*, Nature (London) **502**, 207 (2013).
[27] S. Michimasa *et al.*, Phys. Rev. Lett. **121**, 022506 (2018).
[28] H. N. Liu *et al.*, Phys. Rev. Lett. **122**, 072502 (2019).
[29] M. Enciu *et al.*, Phys. Rev. Lett. **129**, 262501 (2022).
[30] P. J. Li *et al.*, Phys. Lett. B **855**, 138828 (2024).
[31] E. Leistenschneider, E. Dunling, G. Bollen, B. A. Brown, J. Dilling, A. Hamaker, J. D. Holt, A. Jacobs, A. A. Kwiatkowski, T. Miyagi, W. S. Porter, D. Puentes, M. Redshaw, M. P. Reiter, R. Ringle, R. Sandler, C. S. Sumithrarachchi, A. A. Valverde, and I. T. Yandow (LEBIT and TITAN Collaborations), Phys. Rev. Lett. **126**, 042501 (2021).

[32] D. Steppenbeck *et al.*, Phys. Rev. C **96**, 064310 (2017).
[33] D.-C. Dinca *et al.*, Phys. Rev. C **71**, 041302(R) (2005).
[34] S. Iimura *et al.*, Phys. Rev. Lett. **130**, 012501 (2023).
[35] S. Zhu *et al.*, Phys. Rev. C **74**, 064315 (2006).
[36] R. F. Garcia Ruiz *et al.*, Nat. Phys. **12**, 594 (2016).
[37] B. A. Brown, Physics **4**, 525 (2022).
[38] J. Bonnard, S. M. Lenzi, and A. P. Zuker, Phys. Rev. Lett. **116**, 212501 (2016).
[39] L. A. Riley, M. L. Agiorgousis, T. R. Baugher, D. Bazin, M. Bowry, P. D. Cottle, F. G. DeVone, A. Gade, M. T. Glowacki, K. W. Kemper, E. Lunderberg, D. M. McPherson, S. Noji, F. Recchia, B. V. Sadler, M. Scott, D. Weisshaar, and R. G. T. Zegers, Phys. Rev. C **90**, 011305(R) (2014).
[40] FRIB Decay Station initiator proposal, https://fds.ornl.gov/wp-content/uploads/2020/09/FDSi-Proposal-May2020.pdf (2020).
[41] FRIB Decay Station initiator, https://fds.ornl.gov/initiator/ (2023).
[42] S. V. Paulauskas, M. Madurga, R. Grzywacz, D. Miller, S. Padgett, and H. Tan, Nucl. Instrum. Methods Phys. Res., Sect. A **737**, 22 (2014).
[43] W. A. Peters *et al.*, Nucl. Instrum. Methods Phys. Res., Sect. A **836**, 122 (2016).
[44] M. Karny, K. P. Rykaczewski, A. Fijałkowska, B. C. Rasco, M. Wolińska-Cichocka, R. K. Grzywacz, K. C. Goetz, D. Miller, and E. F. Zganjar, Nucl. Instrum. Methods Phys. Res., Sect. A **836**, 83 (2016).
[45] M. Karny, A. Fijałkowska, R. K. Grzywacz, B. C. Rasco, K. P. Rykaczewski, and M. Stepaniuk, Nucl. Instrum. Methods Phys. Res., Sect. B **463**, 390 (2020).
[46] R. Yokoyama *et al.*, Nucl. Instrum. Methods Phys. Res., Sect. A **937**, 93 (2019).
[47] M. Singh, R. Yokoyama, R. Grzywacz, A. Keeler, T. King, J. Agramunt, N. Brewer, S. Go, J. Liu, S. Nishimura, P. Parkhurst, V. Phong, M. Rajabali, B. Rasco, K. Rykaczewski, D. Stracener, A. Tolosa-Delgado, K. Vaigneur, and M. Wolińska-Cichocka, Nucl. Instrum. Methods Phys. Res., Sect. A **1703**, 170239 (2025).
[48] H. L. Crawford *et al.*, Phys. Rev. Lett. **129**, 212501 (2022).
[49] T. J. Gray *et al.*, Phys. Rev. Lett. **130**, 242501 (2023).
[50] I. Cox *et al.*, Phys. Rev. Lett. **132**, 152503 (2024).
[51] P. F. Mantica, R. Broda, H. L. Crawford, A. Damaske, B. Fornal, A. A. Hecht, C. Hoffman, M. Horoi, N. Hoteling, R. V. F. Janssens, J. Pereira, J. S. Pinter, J. B. Stoker, S. L. Tabor, T. Sumikama, W. B. Walters, X. Wang, and S. Zhu, Phys. Rev. C **77**, 014313 (2008).
[52] H. L. Crawford, R. V. F. Janssens, P. F. Mantica, J. S. Berryman, R. Broda, M. P. Carpenter, N. Cieplicka, B. Fornal, G. F. Grinyer, N. Hoteling, B. P. Kay, T. Lauritsen, K. Minamisono, I. Stefanescu, J. B. Stoker, W. B. Walters, and S. Zhu, Phys. Rev. C **82**, 014311 (2010).
[53] R. Grzywacz *et al.*, Phys. Rev. Lett. **81**, 766 (1998).
[54] A. Poves, J. Sánchez-Solano, E. Caurier, and F. Nowacki, Nucl. Phys. **A694**, 157 (2001).
[55] M. Honma, T. Otsuka, B. A. Brown, and T. Mizusaki, Eur. Phys. J. A **25**, 499 (2005).
[56] A. Magilligan, B. A. Brown, and S. R. Stroberg, Phys. Rev. C **104**, L051302 (2021).
[57] L. Coraggio, G. De Gregorio, A. Gargano, N. Itaco, T. Fukui, Y. Z. Ma, and F. R. Xu, Phys. Rev. C **102**, 054326 (2020).
[58] L. Coraggio, G. De Gregorio, A. Gargano, N. Itaco, T. Fukui, Y. Z. Ma, and F. R. Xu, Phys. Rev. C **104**, 054304 (2021).
[59] H. Hergert, S. K. Bogner, T. D. Morris, A. Schwenk, and K. Tsukiyama, Phys. Rep. **621**, 165 (2016), Memorial Volume in Honor of Gerald E. Brown.
[60] S. R. Stroberg, H. Hergert, S. K. Bogner, and J. D. Holt, Annu. Rev. Nucl. Part. Sci. **69**, 307 (2019).
[61] S. R. Stroberg, https://github.com/ragnarstroberg/imsrg (2023).
[62] N. Shimizu, T. Mizusaki, Y. Utsuno, and Y. Tsunoda, Comput. Phys. Commun. **244**, 372 (2019).
[63] T. Koiwai *et al.*, Phys. Lett. B **827**, 136953 (2022).
[64] B. A. Brown, D. B. Fossan, J. M. McDonald, and K. A. Snover, Phys. Rev. C **9**, 1033 (1974).
[65] A. F. Lisetskiy, B. A. Brown, M. Horoi, and H. Grawe, Phys. Rev. C **70**, 044314 (2004).
[66] J. Blomqvist and A. Molinari, Nucl. Phys. **A106**, 545 (1968).
[67] R. F. Garcia Ruiz, M. L. Bissell, K. Blaum, N. Frömmgen, M. Hammen, J. D. Holt, M. Kowalska, K. Kreim, J. Menéndez, R. Neugart, G. Neyens, W. Nörtershäuser, F. Nowacki, J. Papuga, A. Poves, A. Schwenk, J. Simonis, and D. T. Yordanov, Phys. Rev. C **91**, 041304(R) (2015).
[68] R. du Rietz, J. Ekman, D. Rudolph, C. Fahlander, A. Dewald, O. Möller, B. Saha, M. Axiotis, M. A. Bentley, C. Chandler, G. de Angelis, F. Della Vedova, A. Gadea, G. Hammond, S. M. Lenzi, N. Mărginean, D. R. Napoli, M. Nespolo, C. Rusu, and D. Tonev, Phys. Rev. Lett. **93**, 222501 (2004).
[69] J. M. Allmond, B. A. Brown, A. E. Stuchbery, A. Galindo-Uribarri, E. Padilla-Rodal, D. C. Radford, J. C. Batchelder, M. E. Howard, J. F. Liang, B. Manning, R. L. Varner, and C.-H. Yu, Phys. Rev. C **90**, 034309 (2014).
[70] T. J. Gray *et al.*, Phys. Lett. B **855**, 138856 (2024).
[71] W. A. Richter, S. Mkhize, and B. A. Brown, Phys. Rev. C **78**, 064302 (2008).
[72] M. Dufour and A. P. Zuker, Phys. Rev. C **54**, 1641 (1996).
[73] D. D. Dao and F. Nowacki, Phys. Rev. C **105**, 054314 (2022).
[74] E. Caurier, F. Nowacki, and A. Poves, Phys. Rev. C **90**, 014302 (2014).
[75] A. Poves, F. Nowacki, and Y. Alhassid, Phys. Rev. C **101**, 054307 (2020).
[76] H. L. Crawford *et al.*, Phys. Rev. Lett. **110**, 242701 (2013).
[77] F. Nowacki, A. Poves, E. Caurier, and B. Bounthong, Phys. Rev. Lett. **117**, 272501 (2016).
[78] http://energy.gov/downloads/doe-public-access-plan.
[79] T. Miyagi, Eur. Phys. J. A **59**, 150 (2023)..
[80] T. H. Ogunbeku *et al.*, arXiv:2506.21852.

End Matter

TABLE II. Comparison of experimental $E2$ strengths of fp-shell nuclei near $N = 32$, 34 [9,33,63,67] to theoretical predictions using the UFP-CA interaction with adopted effective charges, $e_\pi = 1.30e$, $e_\nu = 0.452e$. The same quantities are compared for ^{50}Ti ($N = 28$) and ^{51}Fe/^{51}Mn ($N \approx Z$) [68–70], using the GXPF1A interaction. The $E2$ matrix element, $\langle J_f^\pi || E2 || J_i^\pi \rangle = M_p$, is related to the transition probabilities through the expression $B(E2) = M_p^2/(2J_i + 1)$, where $M_p = A_p e_\pi + A_n e_\nu$.

		Experiment		Theory (UFP-CA)			
Isotope	$J_i^\pi \rightarrow J_f^\pi$	$B(E2)$ [W.u.] or Q_s [eb]	$M(E2)$ [efm^2]	A_p [efm^2]	A_n [efm^2]	$M(E2)$ [efm^2]	$B(E2)$ [W.u.] or Q_s [eb]
^{49}Ca	$(3/2)^-_{\mathrm{g.s}}$	−0.036(3)	−5.08(42)	0	−12.31	−5.56	−0.039
^{50}Ca	$2_1^+ \rightarrow 0_1^+$	0.68(2)	6.10(9)	0	13.45	6.08	0.68
^{51}Ca	$(3/2)^-_{\mathrm{g.s}}$	+0.036(12)	5.08(169)	0	11.95	5.40	+0.038
^{55}Ca	$½_1^- \rightarrow (5/2)_1^-$	0.42(18)	3.23(69)	0	5.10	2.30	0.21
^{51}Sc	$(11/2)_1^- \rightarrow (7/2)_1^-$	1.9(5)	16.0(21)	2.90	21.35	13.42	1.34
^{54}Sc	$1_1^+ \rightarrow 3_1^+$	1.93(16)	8.38(35)	3.46	8.47	8.33	1.91
^{54}Ti	$2_1^+ \rightarrow 0_1^+$	6.0(12)	19.1(19)	11.62	10.75	19.96	6.57
χ^2_{norm}							1.1
				Theory (GXPF1A)			
^{50}Ti	$2_1^+ \rightarrow 0_1^+$	6.43(52)	18.76(76)	11.58	10.10	19.61	7.03
^{50}Ti	$4_1^+ \rightarrow 2_1^+$	5.5(15)	23.27(317)	15.90	11.66	25.94	6.83
^{50}Ti	$6_1^+ \rightarrow 4_1^+$	3.14(13)	21.13(44)	13.87	7.73	21.53	3.26
^{51}Mn	$(27/2)_1^- \rightarrow (23/2)_1^-$	4.16(12)	36.18(52)	22.09	17.22	36.50	4.23
^{51}Fe	$(27/2)_1^- \rightarrow (23/2)_1^-$	3.68(21)	34.02(97)	17.22	22.09	32.37	3.33
χ^2_{norm}							1.5